Bendable Nickel Oxide Interfacial Layer via Polydopamine Crosslinking for Flexible Perovskite Solar Cells

Xiaopeng Duan[a,b], Zengqi Huang[a,b], Cong Liu[a,b], Jia Yang[a,b], Licheng Tan[a,b], Yiwang Chen*[a,b]*

X. Duan, Z. Huang, C. Liu, J. Yang, Prof. Dr. L. Tan, Prof. Dr. Y. Chen

[a]College of Chemistry, Nanchang University, 999 Xuefu Avenue, Nanchang 330031, China

[b]Institute of Polymers and Energy Chemistry (IPEC), Nanchang University, 999 Xuefu Avenue, Nanchang 330031, China

Corresponding author. Tel.: +86 791 83968703; Fax: +86 791 83969561; E-mail: ywchen@ncu.edu.cn (Y. C.); tanlicheng@ncu.edu.cn (L. T.).

Author contributions. X. Duan and Z. Huang contributed equally to this work.

Experimental Section

Materials: N, N-dimethylformamide (DMF, 99.8%), dimethyl sulfoxide (DMSO, 99.8%), chlorobenzene (CB, 99.8%), ethyl alcohol (99.5%), bathocuproine (99.99%), nickel nitrate hexahydrate ($Ni(NO_3)_2 \cdot 6H_2O$, 99.999%), dopamine hydrochloride (DA, 98%) and CH_3NH_3I (MAI) were purchased from Sigma-Aldrich and used as received. [6,6]-Phenyl-C_{61}-butyric acid methyl ester ($PC_{61}BM$) were purchased from Xi' an Polymer Light Technology Crop. PbI_2 (99.9985%) was purchased from Alfa Asear.

Preparation of undoped and PDA-doped NiO_x nanoparticle solution: First, 14.54 g $Ni(NO_3)_2 \cdot 6H_2O$ was dissolved in 100 mL deionized water and magnetically stirred for 10 min. Then, 0.4 g/mL NaOH solution was added dropwise to the solution until the pH value reached 10-12. The obtained green emulsion was centrifuged after stirring for 5 min, and the precipitate was washed twice with distilled water and then dried overnight at 80 °C. The obtained green solid small pieces were pulverized and

calcined at 270 °C for 2 h to synthesize a dark black powder as the final product. NiO_x nanoparticles (NPs) were dispersed in deionized water by ultrasonication to prepare a pure NiO_x NPs solution. Finally, the resulting solution was filtered using a polytetrafluoroethylene filter (0.45 μm) and stored for later use. The PDA-doped NiO_x solution was obtained by adding a different mass concentration of dopamine hydrochloride to the dispersed pure NiO_x solution.

Device fabrication: First, the patterned indium tin oxide (ITO) slides were ultrasonically cleaned sequentially in acetone, detergent, distilled water and isopropanol for 15 min and then dried under a stream of nitrogen. The undefiled substrates were treated with oxygen plasma for 3 min prior to coating. Then, undoped and PDA-doped NiO_x films as hole transport layer (HTL) were deposited on ITO substrates by spin casting the nanoparticle solution at 2000 rpm for 30 s and then the films were heated at 120 °C for 30 min. $MAPbI_3$ precursor solution (equimolar CH_3NH_3I and PbI_2 dissolved in DMF/DMSO (9:1 v/v) mixture with total concentration of 2.8 M) was spin coated on the ITO/NiO_x or ITO/NiO_x:PDA substrates with 0 rpm 5 s then 4000 rpm for 25 s. During the last 10 s of the spinning process, the substrate was treated by drop-casting chlorobenzene solvent. After the substrate annealed on a hot stage at 100 °C for 10 min and naturally cooled, PCBM (20 mg/mL in CB) solution was spin-coated on top as an electron transport layer. Then, BCP (0.5 mg/mL) in ethanol absolute was spin-coated at 4500 rpm for 1 min. Finally, a 100 nm thick Ag anode was deposited on the substrate.

Characterization: The particle size distribution of the nanoparticles was measured by a high resolution laser particle size analyzer (Brookhaven 90 Plus PALS). X-ray photoelectron spectroscopy (XPS) and ultraviolet photoelectron spectroscopy (UPS) measurements were performed in an ESCALAB 250Xi, Thermo Fisher (by using Al Kα X-ray source) under high vacuum (10^{-9} mbar). Valence band (VB) measurements were performed by UPS using a bias of 10 V and using Au as a reference. Scanning electron microscopy (SEM) were conducted on SU8020 scanning electron microscope

operated at an acceleration voltage of 8 kV. Atomic force microscopy (AFM) and conductive-AFM images were measured by MultiMode 8-HR (Bruker) atomic force microscope, respectively. A Rigaku D/Max-B X-ray diffractometer with Bragg-Brentano parafocusing geometry was employed to test X-ray diffraction (XRD) patterns. The ultraviolet-visible (UV-Vis) spectra were conducted using a SHIMADZU, UV-2600 spectrophotometer. The water contact angle was measured at a Krüss DSA100s drop shape analyser. The steady-state photoluminescence (PL) and time-resolved photoluminescence (TRPL) spectra were recorded by an Edinburgh instruments FLS920 spectrometer (Edinburgh Instruments Ltd.). To measure the power conversion efficiency, current density-voltage (*J-V*) curves of the devices were measured with a Keithley model 2400 source meter (Abet Solar Simulator Sun2000), equipped with a light source (100 mW cm^{-2}) under AM 1.5 G filter. External quantum efficiency (EQE) values were measured under monochromatic illumination (Oriel Cornerstone 260 1/4 m monochromator equipped with an Oriel 70613NS QTH lamp), and the calibration of the incident light was performed using a monocrystalline silicon diode. The Young's Model studies were measured using the peak-force model of AFM. Mechanical bending was measured by a stepper motor controller (CL-01A).

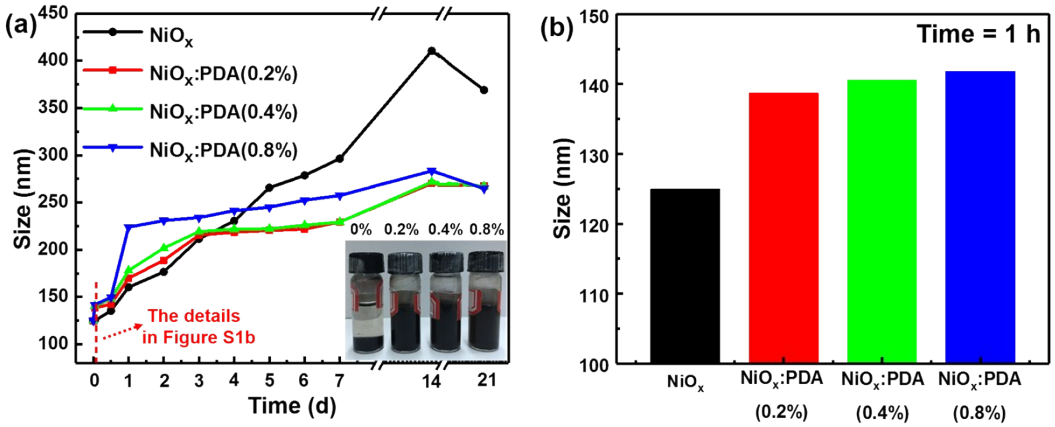

Figure S1. (a) Size distribution of NiO_x:PDA NPs as a function of time upon standing. The inset of (a) shows the photograph of NiO_x:PDA solution upon standing 3 weeks. (b) Size distribution of NiO_x:PDA NPs upon standing 1 h.

In the long-term measurement, the original solution exhibited a faster rate of particle size growth compared to the PDA-doped nanoparticle solution (**Fig. S1a)**, which inevitably affected the uniformity and flatness of the film. More importantly, the original solution existed obvious aggregation after two weeks and it completely precipitated within three weeks, while the modified solution remained stable with excellent dispersibility. As can be seen in **Fig. S1b**, the particle size of NPs increased significantly, which was resulted from naturally self-polymerized PDA binding to NiO_x within short time.

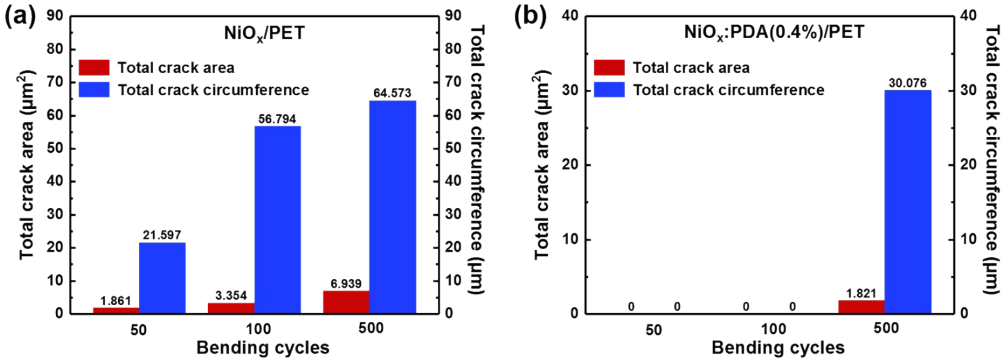

Figure S2. The total area and total circumference of the cracks in SEM images calculated from by AutoCAD software.

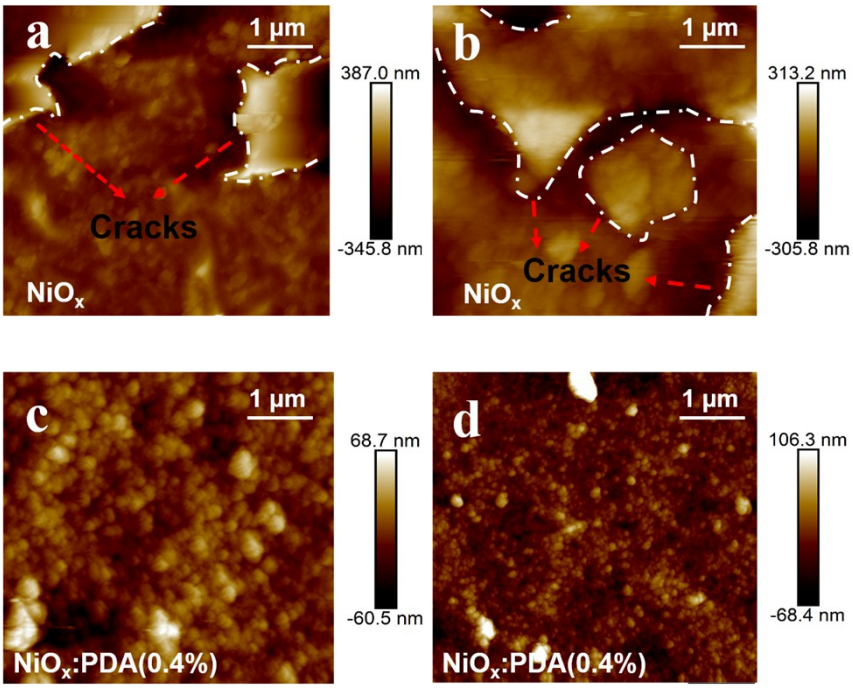

Figure S3. Typical AFM images of unmodified NiO_x and NiO_x:PDA (0.4%) films under different bending times: (a, c) 50 times, and (b, d) 500 times.

The surface of NiO_x/PET shows more cracks after 50 bending times, and a large amount of NiO_x fall off to form separate regions. The NiO_x:PDA (0.4%)/PET film shows only a slight increase in roughness, while the surface remains intact, which is in consistent with the SEM results.

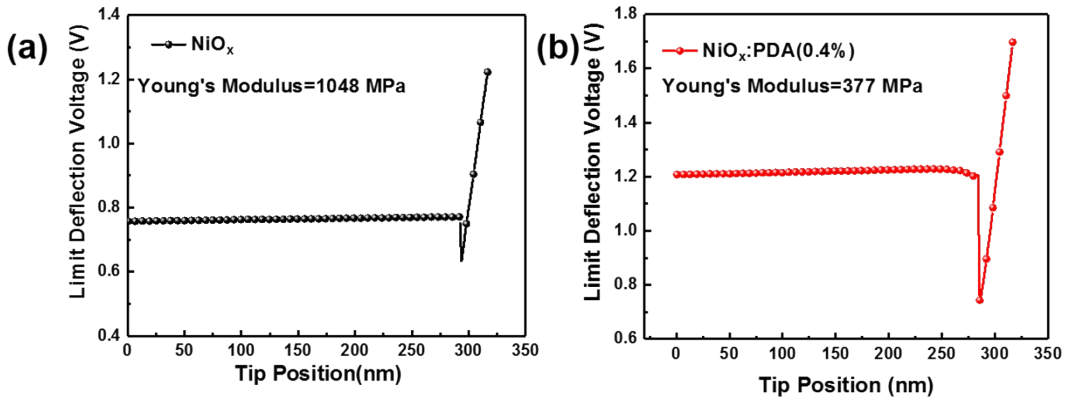

Figure S4. Young's modulus of NiO_x and NiO_x:PDA films.

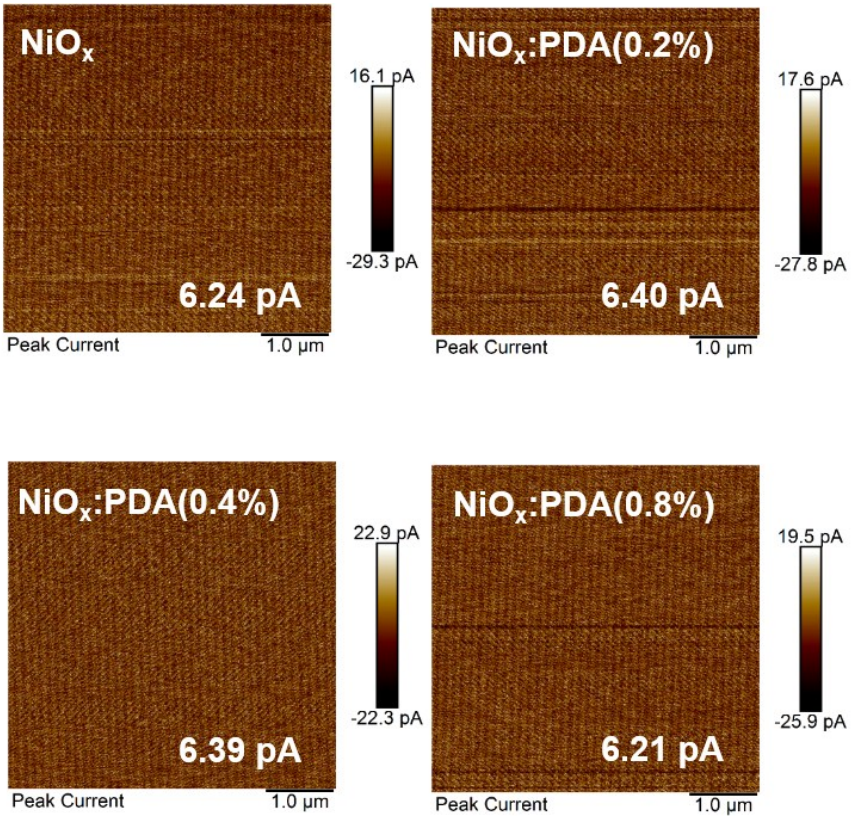

Figure S5. Conductive-AFM characteristics of NiO_x and NiO_x:PDA films coated on ITO substrate. The scan size is 5 μm × 5 μm.

The average current and conductive area distribution of NiO_x and NiO_x:PDA films are observed via conductive AFM. It is worth mentioning that the conductive regions of the NiO_x film are still uniform, indicating that the conductivity is not weakened due to the absence of aggregation for insulating PDA.

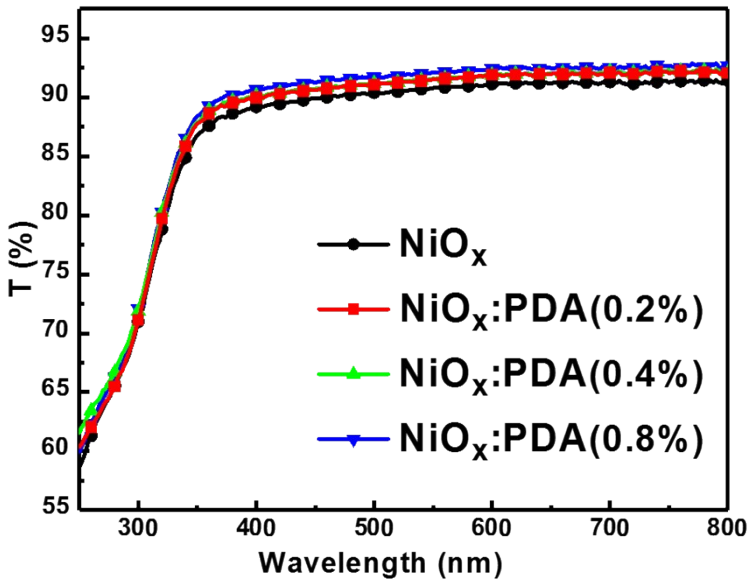

Figure S6. Transmission spectra of NiO_x:PDA films (20 nm) coated on quartz after thermal annealing.

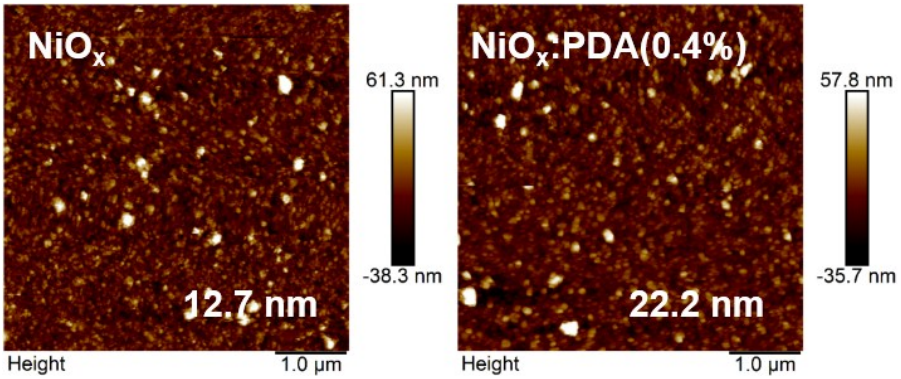

Figure S7. AFM images for NiO_x films and NiO_x:PDA films coated on ITO substrate.

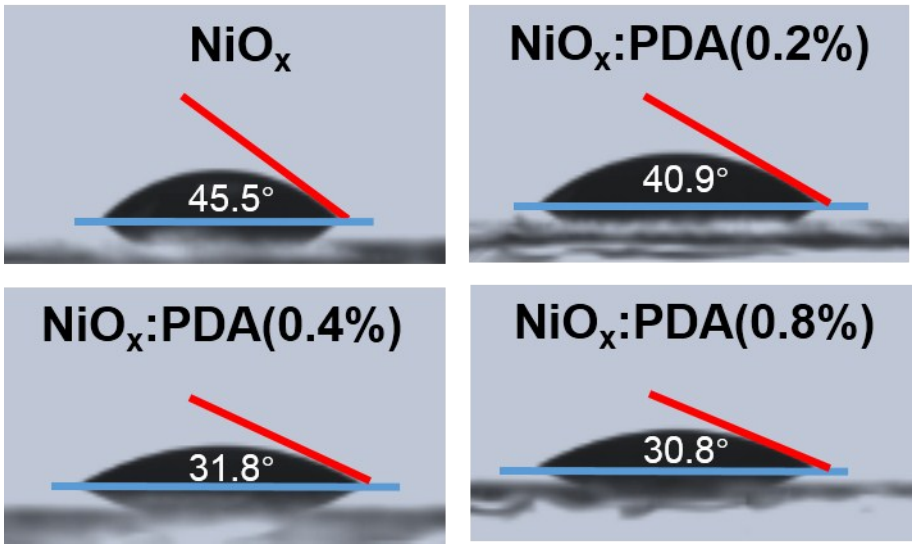

Figure S8. Contact angles of NiO_x and NiO_x:PDA films.

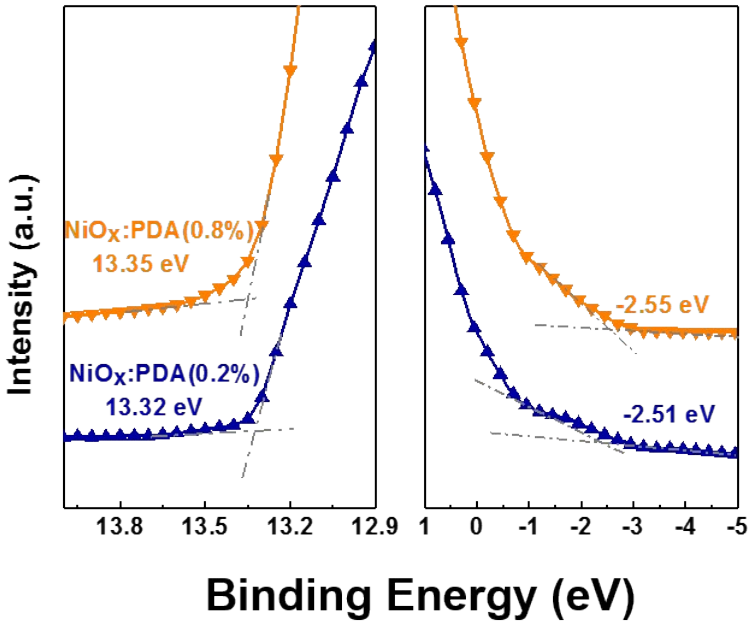

Figure S9. Ultraviolet photoelectron spectroscopy (UPS) of NiO_x:PDA (0.2%) and NiO_x:PDA (0.8%) films coated on ITO glass, measured under -10 eV bias.

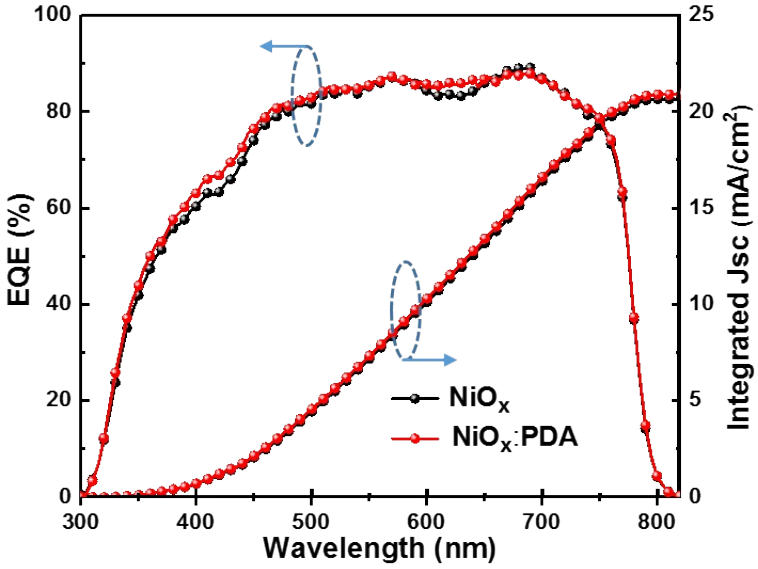

Figure S10. The external quantum efficiency (EQE) spectra of the devices based on the structure of ITO/NiO_x(w/o and with 0.4 wt% PDA)/$MAPbI_3$/PCBM/BCP/Ag.

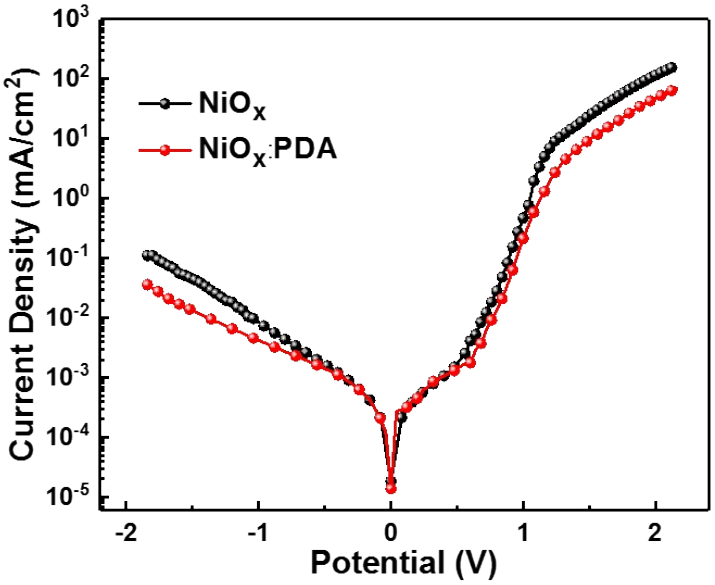

Figure S11. Dark *J-V* curves of PVSCs devices based on ITO/NiO_x (w/o and with 0.4 wt% PDA)/$MAPbI_3$/PCBM/BCP/Ag.

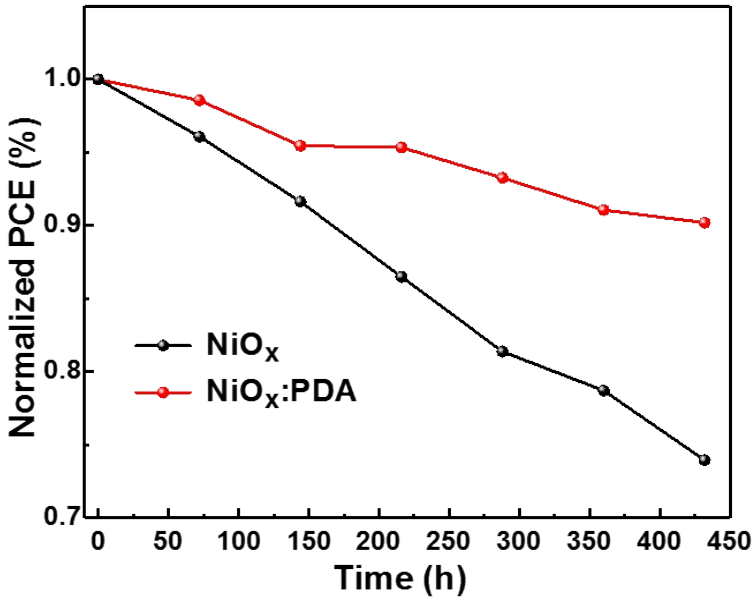

Figure S12. The long-term stability of PVSCs devices based on ITO/NiO_x (w/o and with 0.4 wt% PDA)/$MAPbI_3$/PCBM/BCP/Ag.

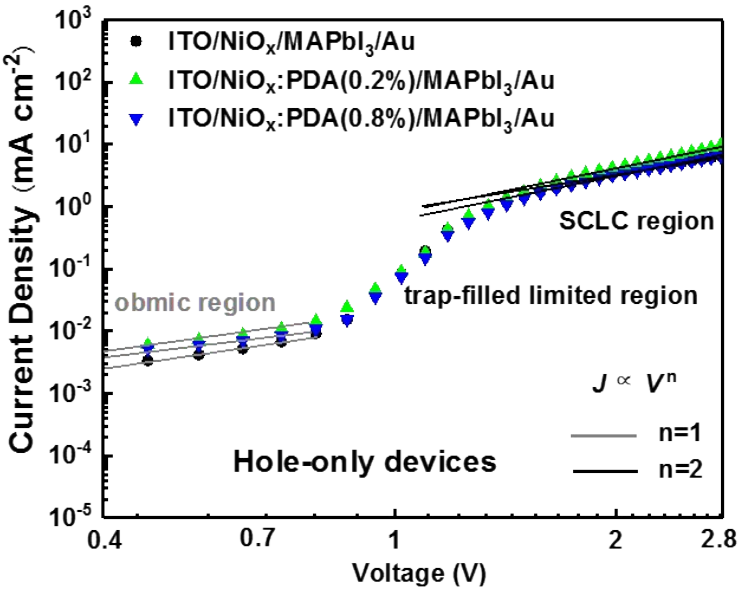

Figure S13. The current density-voltage (*J-V*) curves of the hole-only devices based on ITO/NiO_x (w/o or with PDA)/$MAPbI_3$/Au measured by the space charge limited current (SCLC) model.

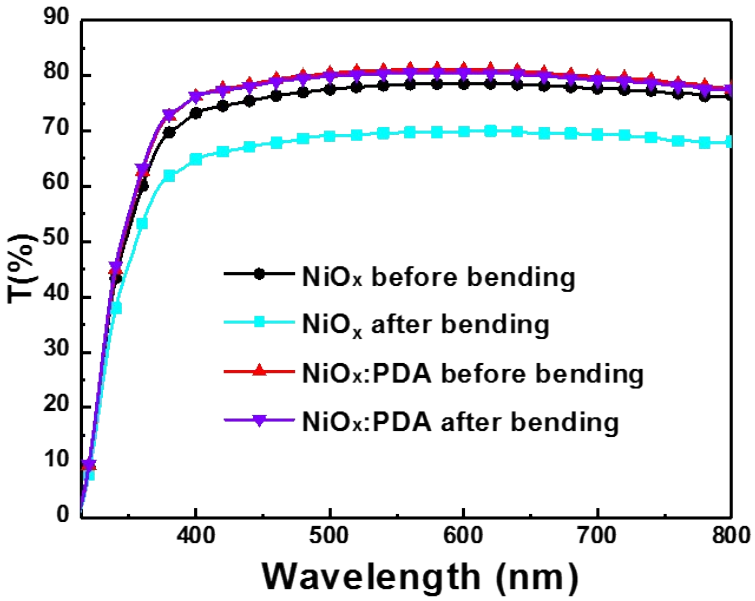

Fig. S14 The transmittance spectra of NiO_x and NiO_x:PDA on PET substrate before and after bending 500 times.

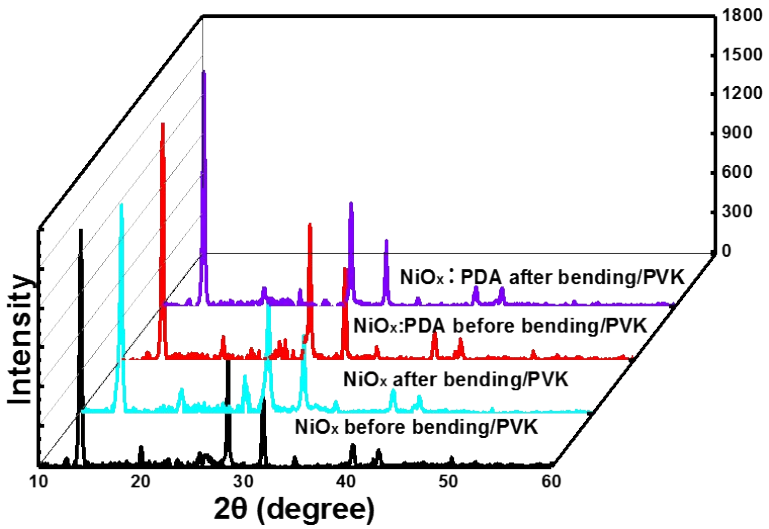

Fig. S15 XRD patterns of perovskite films coated on the PET/NiO_x or PET/NiO_x:PDA substrate. A portion of substrates have been previously bent 500 times.

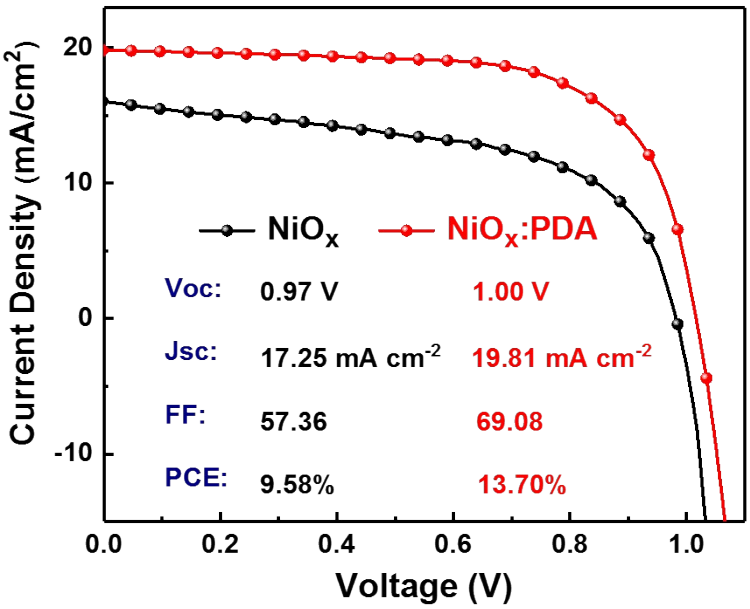

Figure S16. *J-V* curves of flexible perovskite solar cells based on NiO_x and NiO_x:PDA (0.4 wt%) hole-transport layers.

Table S1. The proportion of different forms of Ni in NiO_x:PDA calculated by XPS peak fitting.

Sample	Ni^{2+}	Ni^{3+}	Ni-N	
NiO_x	45%	55%	-	
NiO_x:PDA(0.2%)	45%	55%	-	
NiO_x:PDA(0.4%)	44%	51%	5%	
			From Ni^{2+}	From Ni^{3+}
			1%	4%
NiO_x:PDA(0.8%)	43%	48%	9%	
			From Ni^{2+}	From Ni^{3+}
			2%	7%

The Ni-N interaction not only causes a significant shift in the Ni^{3+} state and Ni^{2+} state characteristic peaks to a higher electron binding energy direction, but also produces a new Ni-N peak. This phenomenon is commonly observed in XPS profiles for Ni elements.[1-2] The Ni^{2+} and Ni^{3+} state proportion decrease as the PDA concentration increases. Therefore, we suspect that the emergence of the new peak is due to the formation of a higher valence state of Ni which is ascribed from Ni^{2+} and Ni^{3+} bonding to N. Moreover, since NiO_x is a mixture of three components (NiO, NiOOH, and Ni_2O_3), and the components are difficult to convert each other, we believe that the new Ni-N state characteristic peak is also a composite peak, including a plurality of sub-peaks. When the concentration of PDA increases from 0.4% to 0.8%, the bonding ratio of Ni^{3+} to N is about 3%, which is more than that of Ni^{2+}, so the composite peak necessarily moves toward the center of the Ni^{3+}-N sub-peak.

Table S2. Fitted parameters for the time-resolved photoluminescence (TRPL) decay measurements.

HTLs	τ_1 (ns)	Fraction (A_1)	τ_2 (ns)	Fraction (A_2)
NiO_x	6.2	19.7	72.9	80.3
NiO_x:PDA(0.2%)	3.9	20.8	45.8	79.2
NiO_x:PDA(0.4%)	2.9	28.2	25.3	71.8
NiO_x:PDA(0.8%)	3.0	31.7	21.3	68.3

The lifetime was obtained by fitting the TRPL spectra measured from the perovskite films with a bi-exponential decay function of the form:[3]

$$I(t) = A_1 \exp(-\tau/\tau_1) + A_2 \exp(-\tau/\tau_2)$$

Table S3. The valence band (VB) values of NiO_x with or w/o PDA modification.

HTLs	$E_{cut-off}$ (eV)	E_{oneset} (eV)	VB (eV)
NiO_x	13.22	-2.82	-5.18
NiO_x:PDA (0.2%)	13.32	-2.51	-5.32
NiO_x:PDA (0.4%)	13.31	-2.56	-5.35
NiO_x:PDA (0.8%)	13.35	-2.55	-5.39

Table S4. The carrier mobilities and corresponding defect densities of hole-only devices based on NiO_x and NiO_x:PDA.

Device	Hole mobility[a] ($cm^2 V^{-1} s^{-1}$)	Defect density (cm^{-3})	Electron mobility[b] ($cm^2 V^{-1} s^{-1}$)
NiO_x	1.77×10^{-5}	3.15×10^{16}	1.19×10^{-4}
NiO_x:PDA(0.2%)	4.22×10^{-5}	2.99×10^{16}	
NiO_x:PDA(0.4%)	4.68×10^{-5}	2.95×10^{16}	
NiO_x:PDA(0.8%)	1.94×10^{-5}	3.12×10^{16}	

Hole mobility[a] measured by the space charge limited current (SCLC) model of the hole-only devices based on the structure of ITO/NiO_x (with or w/o PDA)/$MAPbI_3$/Au. **Electron mobility[b]** measured by the electronic-only devices based on the structure of ITO/SnO_x/$MAPbI_3$/PCBM/BCP/Ag. [4]

Table S5. Photovoltaic performance parameters for the reference PVSCs devices based on ITO/NiO_x/$MAPbI_3$/PCBM/BCP/Ag.

No.	V_{oc} (V)	J_{sc} (mA/cm^2)	FF (%)	PCE (%)
1	0.95	22.48	74.4	15.93
2	0.97	21.83	75.1	15.87
3	1.04	19.91	76.3	15.80
4	0.97	21.90	75.3	15.55
5	0.97	21.90	73.3	15.55
6	0.99	21.67	72.5	15.47
7	1.01	19.05	78.7	15.07
8	1.02	19.75	72.8	14.63
9	1.03	19.14	73.9	14.62
10	1.02	19.39	73.4	14.49
11	1.03	19.63	71.3	14.44
12	0.92	21.85	71.6	14.37
13	1.00	20.02	71.4	14.31
14	1.00	20.10	71.1	14.31
15	1.03	19.44	70.8	14.23
Average	1.00±0.03	20.53±1.23	73.5±2.2	14.98±0.65

Table S6. Photovoltaic performance parameters for PDA incorporated PVSCs devices based on ITO/NiO_x:PDA (0.4%)/$MAPbI_3$/PCBM/BCP/Ag.

No.	V_{oc} (V)	J_{sc} (mA/cm^2)	FF (%)	PCE (%)
1	1.05	22.43	78.1	18.35
2	1.05	22.32	78.0	18.25
3	1.07	22.46	75.4	18.09
4	1.03	22.88	75.9	17.78
5	1.00	22.60	77.2	17.46
6	1.01	21.46	79.4	17.28
7	1.04	21.18	78.2	17.19
8	0.99	22.17	78.5	17.15
9	1.04	21.55	76.2	17.08
10	0.99	22.13	77.6	16.91
11	1.02	20.86	79.2	16.87
12	1.07	20.40	75.7	16.47
13	1.05	20.50	76.0	16.37
14	1.05	20.12	77.3	16.35
15	1.05	20.23	76.8	16.32
Average	1.03±0.03	21.55±0.95	77.3±1.3	17.19±0.68

Table S7. The comparison of PVSCs devices' stability and bendability with the previously studies based on different hole transport layers.

Materials	Device Structure	Bending Curvature (mm)	Bending Cycles	Remaining PCE	Retention Time (h)	Remaining PCE	Year/ Ref.
NiO_x:PDA	ITO/NiO_x:PDA/$MAPbI_3$:PU /PCBM/BCP/Ag	5	1000	73%	432	90%	This work
CuSCN (or NiO_x, Spiro-OMeTAD)	FTO/TiO_2/Perovskite/ CuSCN(or NiO_x or Spiro-OMeTAD)/Au	--	--	--	13	46%, CuSCN 56%, Spiro-OMeTAD 100%, NiO_x	2017[5]
PEDOT:PSS	$AuCl_3$-GR/APTES/PET/ PEDOT:PSS/$MAPbI_3$/ PCBM/BCP/Al	4 (8, 12)	100	90%	<100	99%	2017[6]
NC-PEDOT:PSS	ITO/NC-PEDOT:PSS/ Perovskite/PCBM/BCP/Ag	2	1000	93%	--	--	2018[7]
Spiro-OMeTAD	PET/Graphene/TiO_2/ PCBM/$MAPbI_3$/ Spiro-OMeTAD/CSCNTs	4	2000	84%	1014	92%	2018[8]

References

[1] X. J. Wang, J. Y. Wang, J. Zhang, B. Louangsouphom, J. K. Song, X. Wang and J. F. Zhao, J. Colliod Interf. Sci., 2018, **530**, 1-8.

[2] J. J. Zhu, H. Y. Yin, J. Y. Gong, M. S. H. Al-Furjan and Q. L. Nie, J. Alloy. Compd., 2018, **748**, 145-153.

[3] H. Cho, S.-H. Jeong, M.-H. Park, Y.-H. Kim, C. Wolf, C.-L. Lee, J. H. Heo, A. Sadhanala, N. Myoung, S. Yoo, *Science*, 2015, **350**, 1222-1225.

[4] C. Liu, Z. Q. Huang, X. T. Hu, X. C. Meng, L. Q. Huang, J. Xiong, L. C. Tan and Y. W. Chen, *ACS Appl. Mater. Interfaces*, 2018, **10**, 1909-1916.

[5] J. Cao, H. Yu, S. Zhou, M. C. Qin, T.-K. Lau, X. H. Lu, N. Zhao and C.-P. Wong, *J. Mater. Chem. A*, 2017, **5**, 11071-11077

[6] J. H. Heo, D. H. Shin, M. H. Jang, M. L. Lee, M. G. Kang and S. H. Im, *J. Mater. Chem. A*, 2017, **5**, 21146-21152.

[7] X. T. Hu, Z. Q. Huang, X. Zhou, P. W. Li, Y. Wang, Z. D. Huang, M. Su, M. Z. Li, Y. W. Chen and Y. L. Song, *Adv. Mater.*, 2017, **29**, 1703236.

[8] Q. Luo, H. Ma, Q. Z. Hou, Y. X. Li, J. Ren, X. Z. Dai, Z. B. Yao, Y. Zhou, L. C. Xiang, H. Y. Du, H. C. He, N. Wang, K. L. Jiang, H. Lin, H. W. Zhang and Z. H. Guo, *Adv. Funct. Mater.,* 2018, **28**, 1706777.